J Seismol (2012) 16:131–145
DOI 10.1007/s10950-011-9253-8

ORIGINAL ARTICLE

Improving ShakeMap performance by integrating real with synthetic data: tests on the 2009 M_w=6.3 L'Aquila earthquake (Italy)

Luca Moratto · Angela Saraò

Received: 3 May 2011 / Accepted: 22 September 2011 / Published online: 14 October 2011

Abstract The ShakeMap software automatically generates maps of the peak ground motion parameters (shakemaps) and of instrumental intensity soon after an earthquake. Recorded data are fundamental to obtaining accurate results. In case observations are not available, ShakeMap relies on ground motion predictive equations, but due to unmodelled site conditions or finite fault effects, large uncertainties may appear, mainly in the near-source area where damage is relevant. In this paper, we aim to account for source effects in ShakeMap by computing synthetics to be used for integrating observations and ground motion predictive equations when near-source data are not available. To be effective, the computation of synthetics, as well as of the finite fault, should be done in near real time. Therefore, we computed rapid synthetic seismograms, by a stochastic approach, including the main fault features that were obtained through inversion of regional and teleseismic data. The rapidity of calculation is linked to a number of assumptions, and simplifications that need testing before the procedure can run in automatic mode. To assess the performance of our procedure, we performed a retrospective validation analysis considered as case study of the M_w=6.3 earthquake, which occurred in central Italy on April 6, 2009. In that case, the first shakemaps, generated a few minutes after the earthquake, suffered large uncertainties on ground motion estimates in an area closer to the epicenter due to the lack of near-field data. To verify our approach, we recomputed shakemaps for the L'Aquila earthquake, integrating data available soon after the earthquake at different elapse times with synthetics, and we compared our shaking map with the final shakemap, obtained when all the data were available. Our analysis evidences that (1) when near-source data are missing, the integration of real data with synthetics reduces discrepancies between computed and actual ground shaking maps, mainly in the near-field zone where the damage is relevant and (2) the approach that we adopted is promising in trying to reduce such discrepancies and could be easily implemented in ShakeMap, but some a priori calibration is necessary before running in an automatic mode.

Keywords ShakeMap · Ground motion · Seismic hazard assessment · L'Aquila earthquake · Finite fault · Stochastic seismograms

L. Moratto (✉) · A. Saraò
Centro Ricerche Sismologiche, Istituto Nazionale di Oceanografia e Geofisica Sperimentale (OGS), Borgo Grotta Gigante 42/C, Sgonico, Trieste, Italy
e-mail: lmoratto@inogs.it

A. Saraò
e-mail: asarao@inogs.it

1 Introduction

The ShakeMap software, developed by the U.S. Geological Survey (USGS) Earthquake Hazard

Programs (Wald et al. 1999, 2006), automatically generates maps of the peak ground motion parameters (peak ground acceleration (PGA), peak ground velocity (PGV), and spectral acceleration (SA)) and of instrumental intensity in near real time, after an earthquake. The recorded ground motion parameters (PGMs) are fundamental in order to obtain accurate results. If no observations are available, ShakeMap relies on ground motion predictive equations (GMPEs) and information of site amplifications. Local site amplifications are based on the S-wave velocities in the uppermost 30 m (Vs30), which, as known, suffer from low accuracy (e.g., Wald and Mori 2000; Gallipoli and Mucciarelli 2009).

In Italy, the ShakeMap software has been implemented and customized by the Istituto Nazionale di Geofisica e Vulcanologia (INGV) in the framework of a project financed by the Italian Civil Protection Department (Michelini et al. 2008). The project has also involved a number of other Italian seismological institutions (Istituto Nazionale di Oceanografia e Geofisica Sperimentale–OGS, among the others) that rapidly exchange ground motion parameters in near real time and compute shakemaps in the monitored area.

The main purpose of ShakeMap is to provide maps (hereafter, shakemaps) for post-earthquake response and recovery, other than for public and scientific information; therefore, they must be generated in near real time after the earthquake as their relevance decreases as information about actual damage becomes available. The rapidity of computation can be achieved only by calculating a first-order assessment of the ground shaking. As a consequence, there are multiple sources of uncertainty in producing a shakemaps including sparse ground motion measurements, approximate representation of fault finiteness and directivity, empirical ground motion predictions, numerical interpolation, and site corrections not included (Lin et al. 2005). However, it is possible to associate appropriate levels of confidence to shakemaps as part of their post-earthquake critical decision-making process. Some studies (e.g., Hok and Wald 2003; Lin et al. 2005; Douglas 2007; Bragato 2009) evidenced that, despite the complexity of the matter, requiring consideration of the nominal or dominant frequency content of each input parameter, of the earthquake size (weak versus strong motions), and of the distance to the nearest observations, ShakeMap uncertainties are usually dominated by two aspects: (1) the spatial variability of peak ground motions near recording stations (and thus, station density) and (2) the aleatory uncertainty associated with the GMPE used to estimate the shaking between stations (Lin et al. 2005; Bragato 2009).

Several authors (e.g., Moratto et al. 2009; Ameri et al. 2010) claim the need to integrate recorded data and GMPE with synthetic PGM that account for the main features of the seismic source. In this paper, we propose a procedure to compensate for the lack of real data by accounting for fault finiteness and by adding synthetic PGM rapidly computed including the main features of the source. To validate our approach, we conducted a retrospective analysis, working on a recent well-investigated earthquake as the 2009 (M_w=6.3) L'Aquila event. The L'Aquila real-time shakemaps were computed by INGV, the best that could be based on information available at that time. A critical analysis of how it went and of the possible developments to ameliorate the ShakeMap performance is reported in Faenza et al. (2011) claiming the need of accounting for fault finiteness, and also, Scognamiglio et al. (2010) performed a comprehensive analysis on issues related to the fast seismic source retrieval.

For the purposes of our study, we try to reproduce the final shakemaps—computed some days after the earthquake, when all the data were available at INGV—starting from the data available soon after the earthquake, and including the source effects, first, by simply changing the source approximation and then adding synthetic PGMs. Through the knowledge currently available on the L'Aquila earthquake, we can check whether (1) the gross features of the source rapidly retrieved are meaningful and (2) the algorithm that we adopt to compute synthetic is suitable for our purposes.

2 ShakeMap of the 2009 L'Aquila earthquake

The M_w=6.3 2009 L'Aquila event (L'Aquila earthquake from hereafter) was the first important earthquake, in terms of damage, since the time the ShakeMap software was adopted in Italy. The L'Aquila event occurred on 6 April 2009 at 01:32 UTC in the Central Apennines (Italy) area (lat.=42.33°N, long=13.33°E depth=8.8 km; Faenza et al. 2011) causing nearly 300

casualties and heavy damages in L'Aquila town and in several villages nearby. The earthquake was very well instrumented by the digital permanent seismic stations of the Italian National Seismic Network of INGV (Amato and Mele 2008), by several broadband stations of the MedNet network (Mazza et al. 2008), and by 64 Italian strong motion network (RAN) operated by the National Civil Protection Department (Zambonelli et al. 2011). Seven stations (AQG, AQA, AQV, AQM, AQF, AQP, and AQK) were installed in L'Aquila municipality belonging to the RAN strong motion array of "Valle dell'Aterno" to investigate site effects due to the presence of deep sedimentary basin and shallow sedimentary deposits and to assess the spatial variability of earthquake ground motion (Zambonelli et al. 2011). The "Valle dell'Aterno" array recorded high peaks of accelerations and specifically 0.68 g (AQV), 0.51 g (AQG), 0.49 g (AQA), and 0.37 g (AQK) at a station close to L'Aquila urban area (Zambonelli et al. 2011).

The first shakemaps were generated by INGV about 30 min after the earthquake occurrence (Fig. 1a) including revised epicentral location and data recorded at the INGV stations that did not saturate (Faenza et al. 2011). Where no observations were available, the PGM were computed using the update ShakeMap configuration, that for this earthquake, relies on the GMPE by Akkar and Bommer (2007a, b) (Faenza et al. 2011). The correction factors for site effects are based on a Vs30 classification as described in Michelini et al. (2008).

Shakemaps were updated as new recorded data become available, but it took several hours beforehand to get the shaking maps computed with all the observations (Fig. 1b). The main source of problem regarded the data availability: the INGV broadband stations were saturated at a distance of about 80–90 km from the epicenter; the data transmission for the on-demand strong motion stations failed and the RAN data were (and are) not delivered in real time to INGV (Faenza et al. 2011).

As a matter of fact, the maps generated immediately after the earthquake (Fig. 1a) and the final shakemaps, published several days after the main shock including all the available data and the finite fault from Global Positioning System (GPS) inversion, show big differences—about 20%g in near-source zone with a maximum of 40%g at the stations placed above the rupture area (Faenza et al. 2011)—just in the zone affected by more damages and casualties.

In this paper, for the purposes of our analysis, we recomputed the starting and final shakemaps using data provided by INGV. In our final shakemap

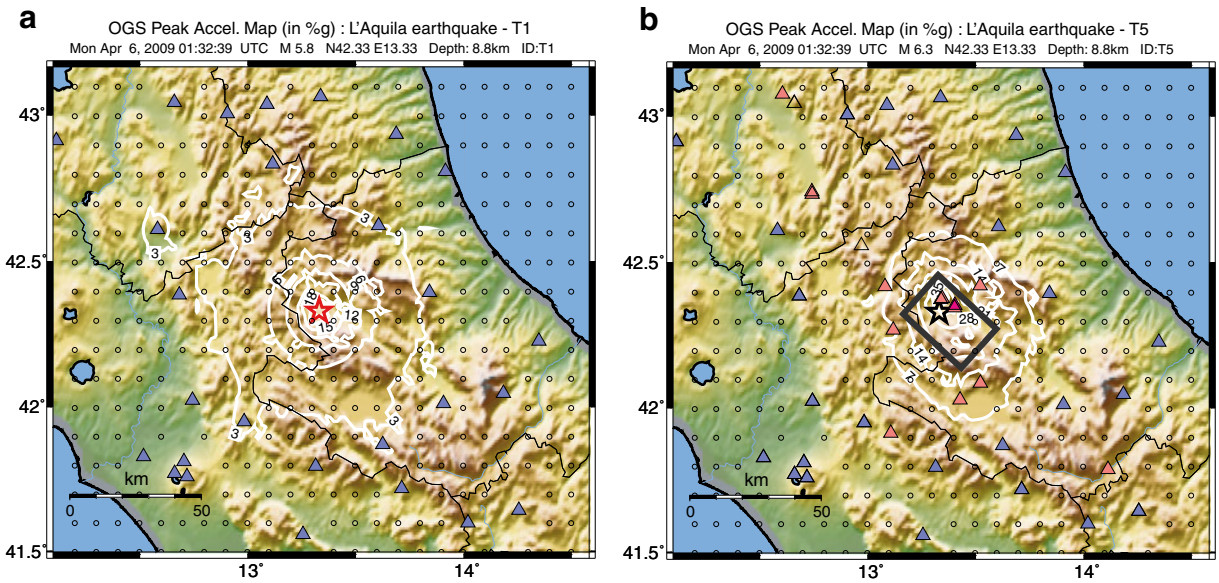

Fig. 1 Shakemap computed within this study using **a** data recorded at INGV stations (*blue triangles*) in test T1. Max PGA, around 20%g. **b** Data recorded at INGV (*blue triangles*) and RAN stations (*red triangles*) in test T5. Max PGA, around 60%g. The source box parameters are those retrieved in this paper (Section 3)

(Fig. 1b), we adopted the fault geometry as obtained within this study. Since in this case data are dominating, the small variations in fault dimension have little relevance in the shakemap computation, and the differences between our shakemaps and INGV final shakemaps (Faenza et al. 2011) are barely visible.

3 The 2009 L'Aquila seismic source

Several studies have currently been published about the source model of the L'Aquila earthquake, starting from the revision of the first moment tensor solutions (Pondrelli et al. 2010; Scognamiglio et al. 2010; Herrmann et al. 2011). The main shock ruptured a normal fault striking along the Apennine axis (NW–SE oriented) and dipping toward the South–West, at nearly 50°. The city of L'Aquila lies a few kilometers away on the hanging wall.

The identification of the fault geometry relied on the aftershock pattern, on the SAR interferometric data (Atzori et al. 2009) on the GPS displacements (Anzidei et al. 2009) as well as on field data of coseismic ground deformation (Boncio et al. 2010). The rupture history obtained from nonlinear inversion of strong motion and GPS data (Cirella et al. 2009) is well correlated with the on-fault aftershock pattern as well as with mapped surface breakages. The significant slip occurred on a segment of about 18 km with a small, shallow patch located updip from the hypocenter and a large, deeper slip patch located southeastward of the rupture nucleation (Cirella et al. 2009). The large slip patch confirms the rupture directivity toward the SE that was observed from the analysis of triggered accelerogram distribution and broadband seismic stations at regional distances (Pino and Di Luccio 2009). The rupture front propagation ranges between 2.2 and 2.8 km/s (Cirella et al. 2009). Poiata et al. (2011), who studied the source process of the 2009 L'Aquila earthquake in both low and broadband frequency ranges using strong motion and broadband modeling of empirical green function, came to similar results. They retrieved the main slip area southeast from the hypocenter with an overall source duration of about 14 s and a rupture velocity estimated at 2.0 km/s.

All of the above information, based on multiple-data inversion and modeling, required some time (days) to be retrieved. Few hours after the earthquake occurrence, the only knowledge about the source was the focal mechanism inferred by moment tensor (e.g., Harvard Global Centroid Moment Tensor (CMT), USGS, MedNet) and some rough slip distribution on the fault gathered from inversion of teleseismic or regional data. For ShakeMap purposes, the latest information, computed in quasi real time, are the only eligible data.

Also at our laboratory, in OGS, we computed the moment tensor and the gross feature of the rupture area in quasi real time using the data recorded by OGS network and teleseismic data from the Incorporated Research Institutions for Seismology (IRIS) data center. Soon after the earthquake, our system computed the moment tensor following the standard procedure based on the Time Domain Moment Tensor algorithm (Dreger 2003) that we use to compute near real-time focal mechanisms of the seismicity (Ml> 3.6) recorded in NE Italy and near surroundings (Saraò 2007; Bragato et al. 2011). Although the station coverage was not optimal, with respect to the source (Fig. 2)—the relation between station coverage and moment tensor solution has been debated in several papers (i.e., Panza and Saraò 2000; Saraò 2007 and references therein)—the energy was well radiated in that direction, and we obtained a solution that fits fairly well with the fast moment tensor computed by USGS, MedNet, and Global CMT Harvard (Fig. 2). Therefore, for this particular earthquake, we adopted the OGS moment tensor solution (strike=130°, dip=46°, and rake=−114°, M_w=6.3) to compute the gross features of the fault model and also because these data were available to us a few minutes after the earthquake. But for the general purpose of validating our procedure, we could have used whatever robust solutions were disseminated by the standard agencies (Harvard Global CMT, USGS). A seismic moment tensor solution robustly computed in real time and a well-calibrated velocity model are mandatory prerequisite. In agreement with the Wells and Coppersmith (1994) empirical relation, a rectangular box model, 25 km long and 15 km wide, was chosen as the plane of the rupture. As data for the slip model, we used teleseismic records downloaded from the IRIS Data System that were available soon after the earthquake. Thirty-one selected teleseismic broadband P-wave data (Fig. 3a), filtered in the range 0.02–0.1 Hz, and a total seismic window of 50 s, were

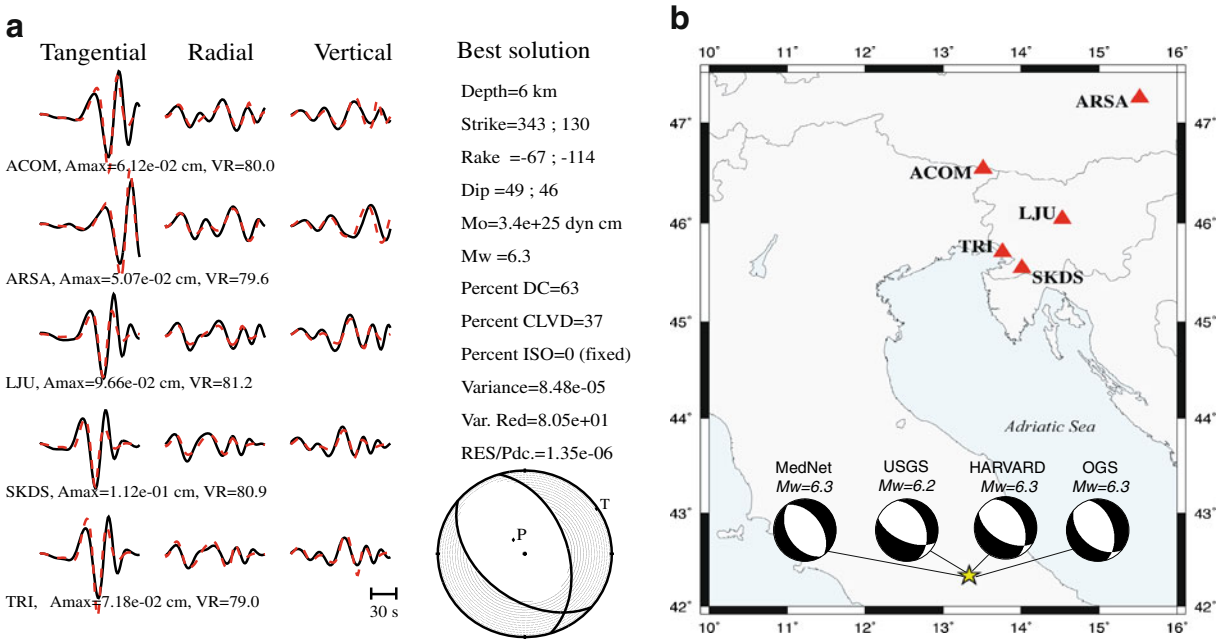

Fig. 2 **a** Moment tensor computed at OGS by TDMT_INV code (Dreger 2003). Waveform fit between real (*black line*) and synthetics (*red line*). The best solution is listed as depth (kilometers), strike, rake, dip, seismic moment (M_0), moment magnitude (M_w), percent of double couple (*DC*), compensated vector linear dipole (*CLVD*), isotropic (*ISO*), variance and variance reduction (*Var. Red*), and the variance divided by the DC percentage (*RES/PDC*). **b** Map of the stations (*triangle*) used for moment tensor inversion in this study. The OGS moment tensor solution is comparable with those obtained in near real time by MedNet, USGS, and CMT Harvard

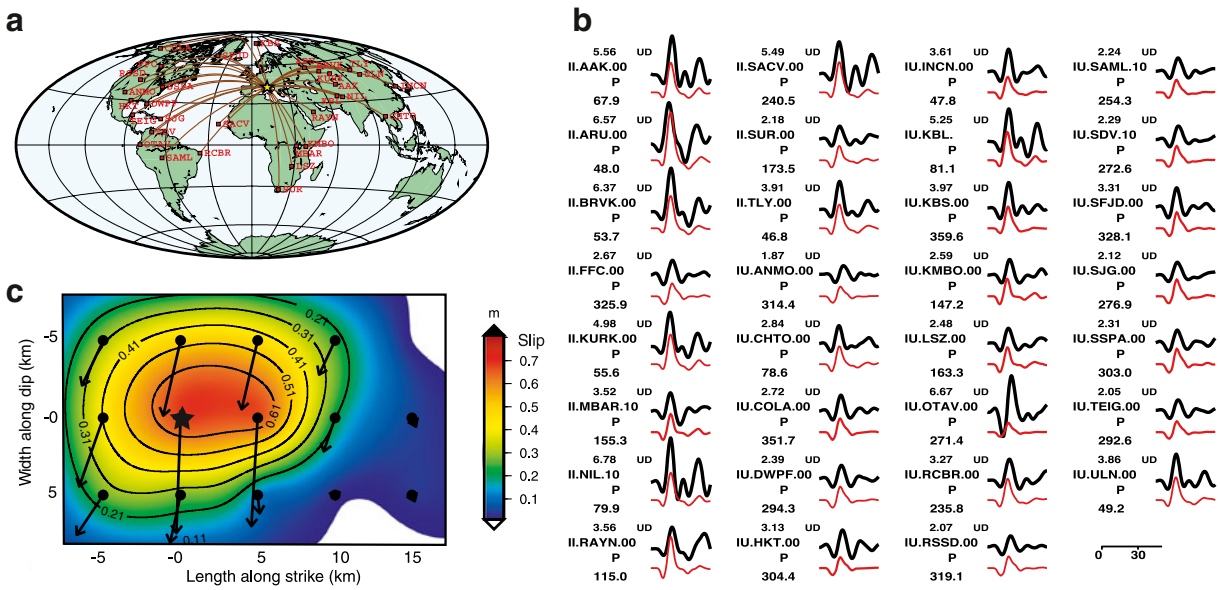

Fig. 3 **a** Global map of the stations used for the teleseismic inversion. **b** Waveform fit between real (*black line*) and synthetics (*red line*) obtained from the inversion for the slip distribution on the fault. For each trace are listed: maximum amplitude (micro-meter) and component, name of the station, phase selected, and azimuth. **c** Gross slip distribution on the fault retrieved in this study over a 5×3 grid mesh. The smooth is obtained within GMT program using the continuous curvature gridding algorithm after processing data to eliminate aliasing using the median method. The *black star* represents the nucleation of the rupture

inverted (Fig. 3b) using the modified Kikuchi and Kanamori (1982, 1993) method, to achieve information about rupture directivity and the position of the fault, with respect to the hypocenter.

The extended source was modeled by 5×3 point sources along the fault, with a separation of 5 km. The rupture velocity was fixed at 2.5 km/s, but other trial inversions were performed in the range 2.4–3.2 km/s with no appreciable changes on the results. For the hypocenter region, a simplified 1D velocity model with four layers was taken from the literature (Parotto et al. 2003 for P-waves and Di Bona et al. 2008 for S-waves and Q), while a global Jeffreys–Bullen model was used for modeling the wave propagation traveling to the receivers.

As rupture plane, having no other kind of constraints when running in real time, we chose the one that minimized the misfit of the inversion. Our best solution has a variance of 0.5 and shows a single asperity, of approximately 18 km, compatible with an unilateral rupture propagation, growing from NW towards SE, found by Cirella et al. (2009). The maximum slip on the fault is about 70 cm, and the source duration is about 13 s (Fig. 3c) consistent with the aforementioned source models. The simplified model resulting from our inversion achieves plausible information related to the position of the rupture plane, with respect to the hypocenter (i.e., directivity) and to the maximum slip on the fault. This outcome could be used as an additional input parameter in ShakeMap prior to computing synthetics. Should we have manipulated some input parameters (i.e., parameterization of the source time function) of the inversion algorithm, we could have probably improved the waveform fit, but this would have worked to the detriment of rapidity without contributing to the improvement of our simplified source model. The time required to get our fault model was almost 1 h, but times can be considerably reduced if the whole procedure would be automized, including the trials to choose among the two nodal planes, based on the waveform fit.

4 Strong motion computation

4.1 The method

We use the algorithm EXSIM (Boore 1983; Motazedian and Atkinson 2005; Boore 2009) and the stochastic finite fault technique to simulate the near-field ground motion records. Numerous studies demonstrated the ability of the method to provide reliable estimates of ground motion in various tectonic environments (e.g., Beresnev and Atkinson 1998; Roumelioti et al. 2004; Castro et al. 2008; Ugurhan and Askan 2010 and references therein).

The EXSIM algorithm is based on the Band-Limited White Noise–Random Vibration Theory (Boore 1983); the ground motions are computed as a time sequence obtained from a band-limited white noise superimposed on a known Fourier amplitude spectrum of the ground motion. The shear-wave amplitude spectrum in the frequency domain is the product of filter functions representing the source, propagation, and site effects. The path effects are modeled through geometrical spreading, anelastic attenuation, and ground motion duration effects (Boore 2005). The simplest approach models the earthquake source as a stochastic point source with ω^2 spectrum (Boore 1983). For large earthquakes, the finite fault approach is adopted in order to account for finite fault effects such as rupture geometry, slip inhomogeneity, and source directivity, which can strongly affect the duration, frequency content, and amplitude of simulated ground motions. Motazedian and Atkinson (2005), Boore (2009), and Atkinson et al. (2009) report in details the differences between point and finite source models in the stochastic approach. In the finite fault approach, the rectangular fault plane is divided into small subfaults, and each subfault is considered to be a point source. The ground motion, contributed by each subfault, is computed by the stochastic point source model (Boore 1983, 2005). The rupture starts at the hypocenter and propagates kinematically until each subfault is triggered. The regional dependence of duration and amplitude on distance are employed in the simulations to model the propagation effects. Finally, the ground motion at a receiver from the entire fault is obtained by summing up the contribution from each subfault with a proper time delay.

To overcome the problems related to the discretization of the fault (i.e., the dependence of the total radiated energy on the subfault size), Motazedian and Atkinson (2005) introduced the dynamic corner frequency approach to scale the high-frequency spectral level of the subfault. Therefore, the corner frequency of the subfaults decreases with time and

then radiated energy at high frequencies also decreases. The high-frequency spectral amplitudes are controlled by stress drop, whereas the percentage of pulsing area defines the level of spectra at low frequencies. Stress drop and percentage of pulsing area are considered "free parameters" and have to be properly calibrated for each study area. Although EXSIM mimics the directivity by the effects of rupture propagation along the fault, it includes also the possibility to use the analytical approach by Mavroeidis and Papageorgiou (2003) to model near-fault pulses that might dominate the signals at long periods due to directivity effects.

4.2 Validation and synthetics

We validate the propagation input parameters used in EXSIM for computing the strong motion of the L'Aquila earthquake through comparisons of simulated and observed acceleration within the frequency range of interest (0.1–25 Hz). As source mechanism, we used the source parameters as described in Section 3. We divided the fault plane into subfaults sized 1×1 km. To account for the geometrical spreading, the anelastic attenuation, and the distance-dependent duration, we employed the parameters for the study area as proposed by Bindi et al. (2009) and the duration model by Herrmann (1985). We roughly assess the site effects at the strong motion stations using the Borcherdt (1994) amplification factors, to mimic the ShakeMap approach, applied to the synthetics computed at bedrock conditions.

To calibrate the stress drop value for the region under investigation, we tried different values of between 40 and 140 bars and then tuned the pulsing percentage value to adjust the lower frequency amplitudes. A fast "trial and error" procedure to tune the stress drop can be developed and implemented in the future. The stress drop of 140 bars is the standard value used in the original version of EXSIM (Atkinson and Boore 2006). That value is greater than the value proposed by Bindi et al. (2009) for the area (about 90 bars), but with a pulsing percentage of 50%, is found to give the best fit between synthetic and recorded Fourier amplitude spectra, PGA and PGV values, respectively.

For validation purposes, the synthetic seismograms were computed within 100 km from the epicenter at 22 accelerometric stations (red triangles in Fig. 1b). The recorded data were downloaded from the ITalian ACcelerometric Archive (ITACA) database (ITACA Working Group 2010) and include the RAN stations of the array "Valle dell'Aterno" (AQA, AQG, AQK, AQU, and AQV). Time histories recorded at those stations are characterized by short duration (less than 10 s) and high peak accelerations (between 0.35 g and 0.65 g) both in the horizontal and vertical directions, although AQK recorded peak vertical accelerations higher than the horizontal ones. The recorded PGA are given in the frequency range 0.05–40 Hz but, since the main energy contribution is within 25 Hz, extracting the PGA values in the frequeny range of synthetics computation (0.1–25 Hz) does not involve significant changes (Fig. 4) except for those stations suffering from site effects (AQG, AQV, AQK). Some authors (e.g., Ameri et al. 2009; Maugeri et al. 2011) found that the amplifications of AQG and AQV could be due to site effects. Maugeri et al. (2011) quantified the PGA amplification factor ranging from about 2.0–2.5. Ameri et al. (2009) claimed that the high value of the vertical component of AQK was probably due to the combination of the source pattern and site effects and that similar considerations apply to other near-source sites. For such cases, the Borcherdt (1994) coefficients, used in ShakeMap to account for site effects, were inadequate as also proved by Barani et al. (2009). Indeed, the comparison (Fig. 5) between

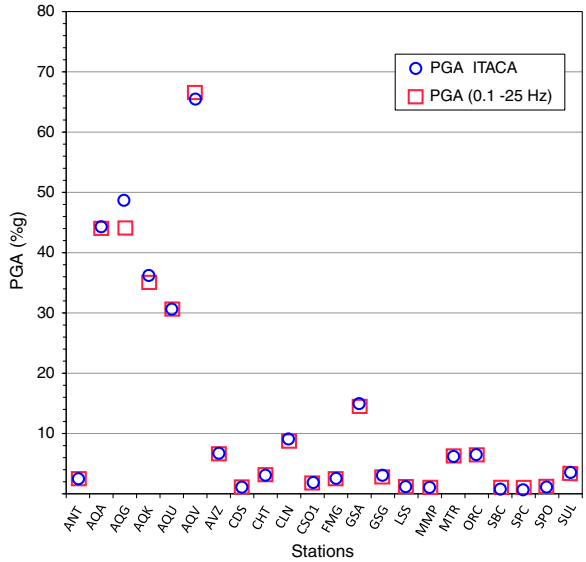

Fig. 4 Observed PGA values extracted in the range 0.05–40 Hz (*blue circle*) and 0.1–25 Hz (*red square*), respectively

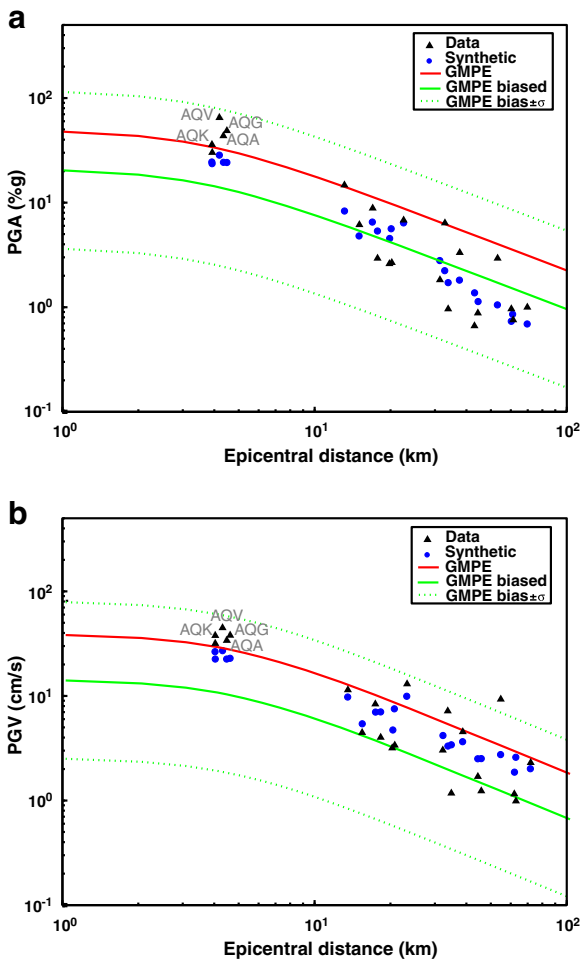

Fig. 5 **a** Comparison between recorded PGA synthetic PGA, GMPE, and biased GMPE. **b** Comparison between recorded PGV, synthetic PGV, GMPE, and biased GMPE

synthetic and real PGA shows that we underestimated the stations above the fault rupture (particularly AQG and AQV) that are within 5 km of the epicenter. However, the bedrock ground motion parameters predicted by the stochastic seismograms are in agreement with the bedrock estimates by Maugeri et al. (2011) who found an average value of 0.3 g at AQG evaluated at the bedrock underlining soil deposits and/or soft rock.

Synthetic data, for places not affected by strong site effects, give results more accurate than GMPEs due also to some effects of finite faults included in the modeling (Fig. 5). At distances larger than 10 km, the synthetic PGMs simulate the PGA distance (Fig. 5a) attenuation shape and the PGV distance attenuation shape (Fig. 5b) better than GMPE. We also compare synthetic PGMs with GMPE, corrected for the bias, that is a correction factor applied in ShakeMap to match the observed data and predicted ground motions accounting for possible errors on magnitude or inter-event variability (Wald et al. 2006).

Both the GMPE (red line) and biased GMPE (green line) underestimate data with strong site effects. The GMPE overestimates PGA at distances greater than 10 km. The biased GMPE (green line) underestimates PGA within 20 km (Fig. 5a) and PGV within 10 km (Fig. 5b), respectively. However, all scattered data are limited within the uncertainties in the GMPE computation for both PGA or PGV. Therefore, GMPE can still be used as a first order of approximation in areas were no a priori knowledge (i.e., about the velocity model) is available and when the implementation with the synthetic data is difficult to be achieved.

5 ShakeMap computations using synthetic data: results and discussion

We computed shakemaps for different magnitude values and source approximations (Table 1) in order to evaluate the sensitivity of shakemaps to different input parameters, and subsequently, we integrated observations with synthetics. For each test, we quantified the differences through a misfit parameter (Table 1) computed as the average of the residuals calculated on each grid node in L2 norm, and we show the spatial variations through differential maps obtained as PGM difference at each grid node.

5.1 Shakemap with data, GMPE, and fault box

At first, we computed two shakemap tests in the point source approximation using only the INGV data. In test T1, we consider the local magnitude Ml=5.8, estimated by INGV soon after the earthquake, while in test T2, we adopted the moment magnitude M_w= 6.3. The difference between the two shakemaps is <5%g (Fig. 6a) near the epicenter zone meaning that the available data, together with the bias factor, were able to minimize the effects due to the magnitude difference. In the further tests, we fixed the magnitude value at M_w=6.3.

The replacement of the point source with the finite fault approximation (test T3) gives an increment of

Table 1 Parameters used in the different study cases named as in the column Code with the related misfit values (percent of gravity)

Code	M_w	Source	INGV stations	RAN stations	AQG/AQV	Synthetic data	Misfit (with T5)	Misfit (with T6)
T1	5.8	Point	x	–	–	–	4.0008	0.8024
T2	6.3	Point	x	–	–	–	3.0426	0.7015
T3	6.3	Finite	x	–	–	–	2.4189	0.4707
T4	6.3	Finite	x	–	–	–	2.4063	0.4615
T5	6.3	Finite	x	x	x	–	0.0000	1.7494
T6	6.3	Finite	x	x	–	–	1.7494	0.0000
S1	6.3	Finite	x	–	–	RAN stations	1.8052	0.1869
S2	6.3	Finite	x	–	–	Grid	2.2339	1.8254
S3	6.3	Finite	x	x	x	Phantom stations	1.8163	0.1881

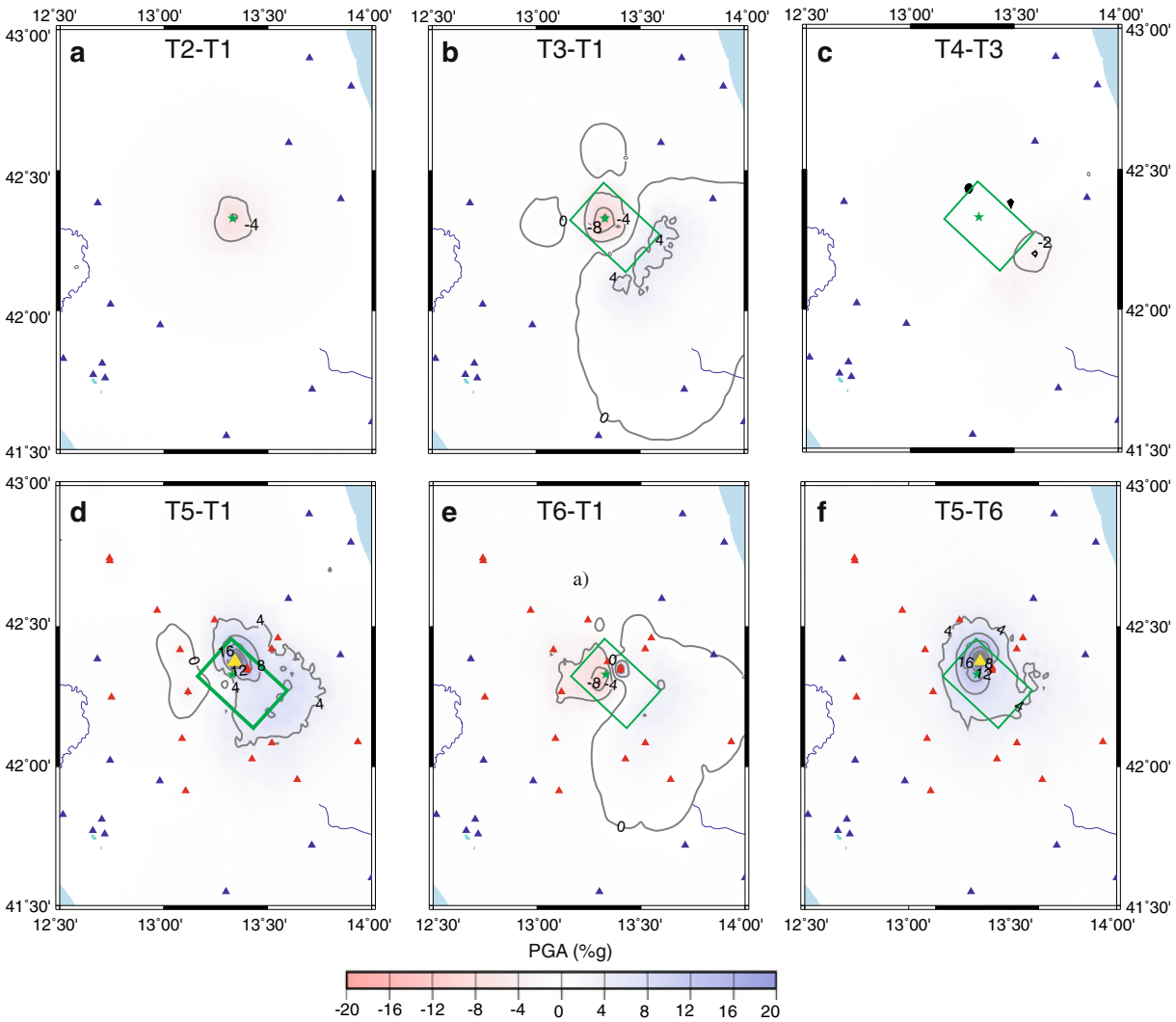

Fig. 6 Differential PGA maps (percent of gravity) between **a** test T2 and test T1, **b** test T3 and test T1, **c** test T4 and test T3, **d** test T5 and test T1, **e** test T6 and test T1, and **f** test T5 and test T6. The *triangles* represent the RAN accelerometric stations (*red*), the INGV broadband stations (*blue*), the AQG and AQV stations (*yellow*), respectively

8%g (Fig. 6b) at the SE end of surface area and a misfit reduction of 40% with respect to the T1 shakemap (Table 1). The finite fault is modeled through a rectangular box placed around the epicenter as resulting from the slip distribution retrieved in this study. We account for the effect of directivity simply by using the station to source distance, computed as epicentral distance in the case of the point source model, and in the Joyner–Boore (R_{JB}) approximation in the case of a finite source. As regards the dimension of the fault, a 5-km reduction on the fault length (test T4) barely affects the shakemap (Fig. 6c), with a maximum difference of 2.5%g observed at the SE end of the fault. In test T5, we computed shakemaps using the fault box, the INGV, and the RAN data (Fig. 1b), while in test T6, we excluded the stations AQG and AQV that recorded the highest acceleration values to verify the changes on the results when strong site effects are absent.

The comparison between the complete shakemaps (test T5) and the shakemaps obtained few minutes after the earthquake occurrence (test T1) shows differences larger than 20%g (PGA_{max} around 40%g) above the rupture plane and larger than 5% g in all the near-source areas (Fig. 6d). If removing AQG and AQV (test 6), we reduce the PGA differences on the rupture plane to an average PGA=10%g and a PGA_{max} around 17%g (Fig. 6e). Indeed, the comparison between tests T5 with T6 (Fig. 6f) shows a maximum difference of 30%g at AQG and AQV sites (yellow triangles in Fig. 6f).

5.2 Shakemap with data, GMPE, fault box, and synthetics

Aiming to verify if synthetics can account for the lack of near-source data, we computed a shakemap integrating the INGV data (test T1) with the finite fault approximation and synthetic PGMs. The computation of the synthetic seismograms required about 15 min.

To start (test S1), we computed synthetic waveforms at the 22 accelerometric stations (red triangles in Fig. 1b), within 100 km from the epicenter, whose data were not transmitted to INGV in real time. Adding synthetics (Fig. 7a, b) in the shakemaps leads to an average misfit reduction of 55% with respect to T1 map, but due to unmodeled site effects, the strong motions just above the rupture area are underestimated (differences larger than 10%g at AQG and AQV sites). Removing AQG and AQV from the observations (test T6), we limit the differences within 5%g above the fault (Fig. 7c), and we improve the average misfit, with respect to T1, up to 77%. The histogram of the percentage PGA residuals (Fig. 7d) confirms that about 10,500 on 15,000 sites differ less than 0.5 between test T6 and test S1.

As a further test, we computed the synthetic seismograms on a regular 0.1° grid placed around the epicenter (test S2). The receivers are located at bedrock sites, within 50 km from the source. We underestimate the PGA in the northern part of the fault (around −5%g) near AQG and AQV, and we overestimate the PGA at the end of the fault (PGA≥ 20%g and PGV≈20 cm/s) where no stations were installed (Fig. 8a, b). The misfit reduction is 44%, and the histogram of the percentage PGA residuals (Fig. 8d) shows that a large number of sites differ less than 10 between test S2 and test T5. However, the absence of real data in a zone where directivity effects are strong can lead to large uncertainties in the shakemaps. The instrumental MCS intensity map (Fig. 9a), derived using the relationship developed for Italy by Faenza and Michelini (2010), displays intensity larger than VIII in the area above the rupture zone. Such a result is satisfactory if qualitatively compared with the values of the macroseismic map (Fig. 9b) taken from the Italian macroseismic database (DBMI08aq 2009).

Finally, (test S3), we estimated the ground motion at the virtual receivers (phantom stations) placed on a regular grid (0.1° sized) within 50 km from the source and used by ShakeMap to evaluate ground motion by GMPEs; the estimated peak values are rejected if there is a recording station within 10 km (Michelini et al. 2008). Adding those synthetics to all the observations (INGV + RAN data) does not produce an evaluable improvement on what can be done using the GMPE. In this case, due to the fine station density, data are predominant, and the contribution of the synthetics at phantom stations has little relevance.

6 Conclusions

Lack of data in the epicentral area produces relevant uncentainties in shakemaps. Through a retrospective analysis, we validate a procedure to reduce ShakeMap

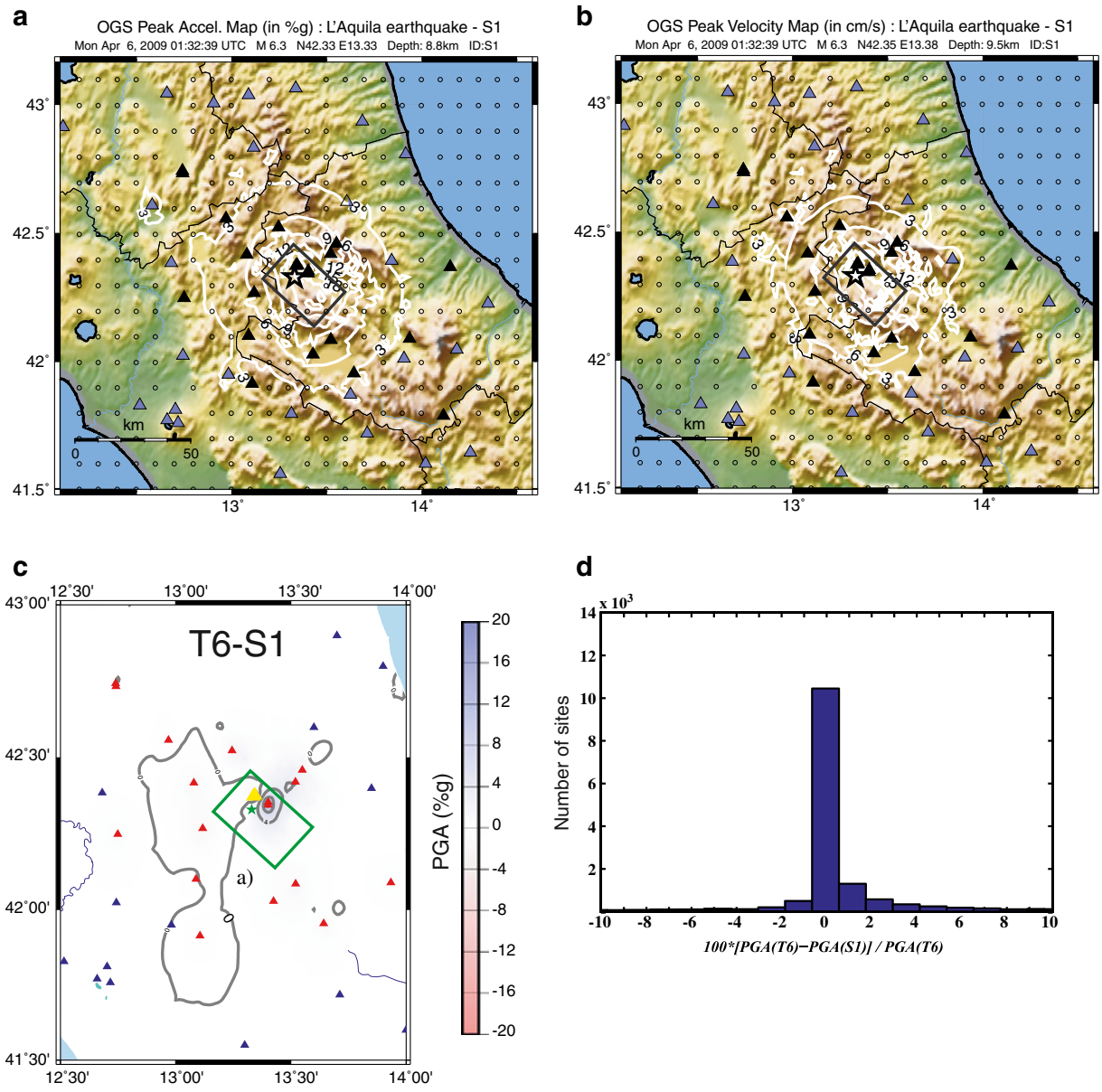

Fig. 7 **a** PGA and **b** PGV shakemaps for test S1 computed using data recorded at INGV stations (*blue triangles*) and synthetic data (*black triangles*). **c** Differential PGA map between test T6 and test S1; *triangles* represent the RAN stations (*red*), the INGV stations (*blue*), and AQG and AQV stations (*yellow*), respectively. **d** Distribution of PGA residuals (T6-S1)/T6. The median value is 0.15

uncertainties by selecting the appropriate input parameters and integrating data with synthetic PGM values. As case study, we chose a well-investigated earthquake, the M_w=6.3 2009 L'Aquila event.

To assess the performance of our approach, we computed shakemaps using all of the pieces of information available at an elapsed time after the occurrence of the earthquake and testing the sensitivity of the shakemaps to different input parameters (magnitude, rupture area, recorded waveforms). Finally, we integrated recorded data with synthetic PGM computed using a stochastic approach that accounts for a simplified fault model, quickly retrieved by waveform inversion of teleseismic data.

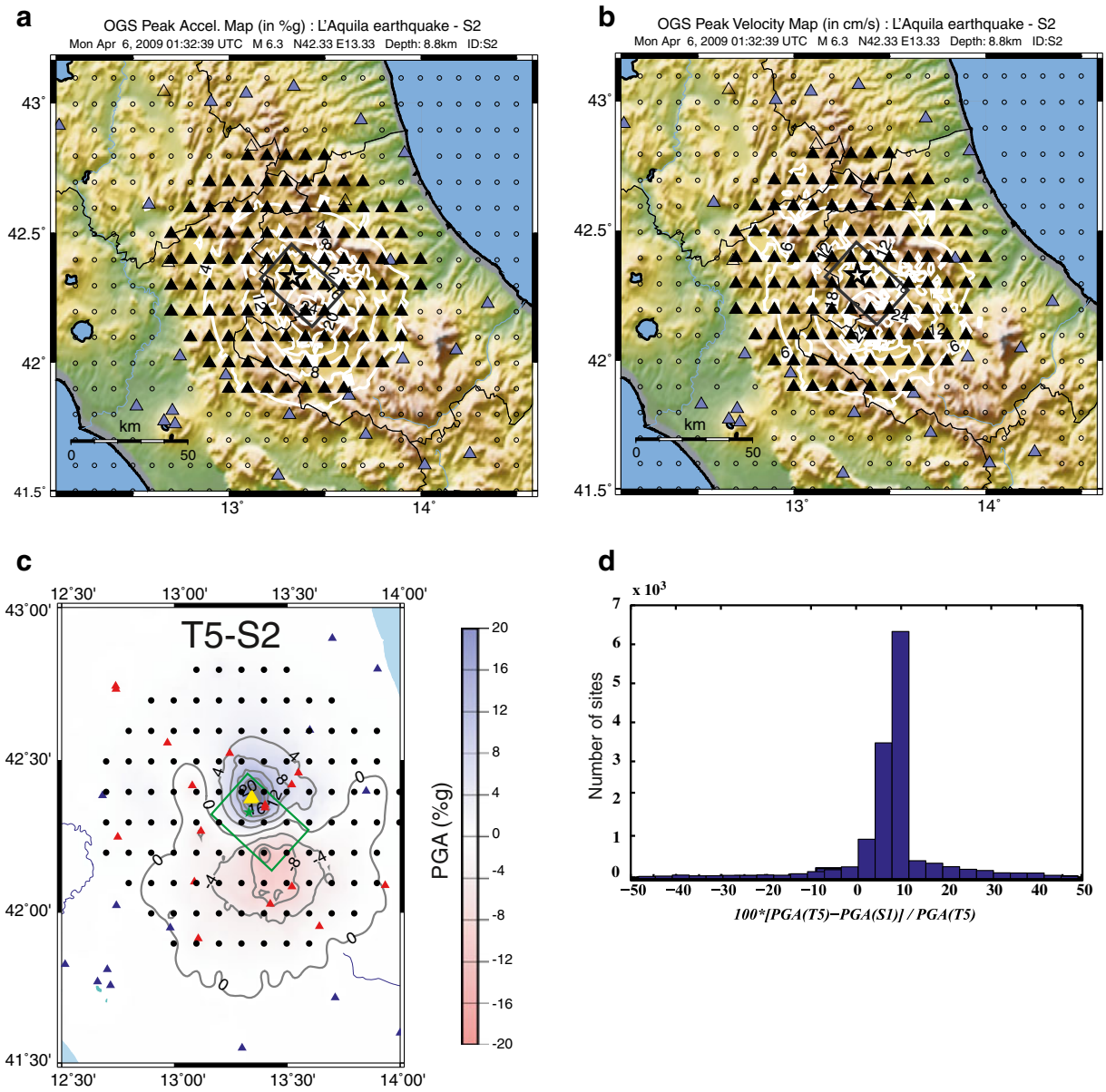

Fig. 8 **a** PGA and **b** PGV shakemaps for test S2 computed using data recorded at INGV (*blue triangles*) and synthetic data (*black triangles*). **c** Differential PGA map between test T5 and test S2; *triangles* show the RAN stations (*red*), the INGV stations (*blue*), and AQG and AQV stations (*yellow*), respectively. **d** Distribution of PGA residuals (T5-S2)/T5. The median value is 8.42

The misfit values related to the comparison of each test with the final shakemap (test T5), obtained when all the data were gathered by INGV, improve as we add more details (M_w, finite box, near-field recordings) to the ShakeMap input. The usage of the finite fault approximation reduces the misfit of 40% with respect to the shakemap computed in the point approximation, while uncertainties (within 5 km) on the dimensions of the rupture area produce negligible effects on the shakemaps. We proved that synthetic PGMs, which include finite source effects, could improve the accuracy of ShakeMap, unless strong site effects exist as, without a priori knowledge, we are not able to reproduce them. Also, synthetics

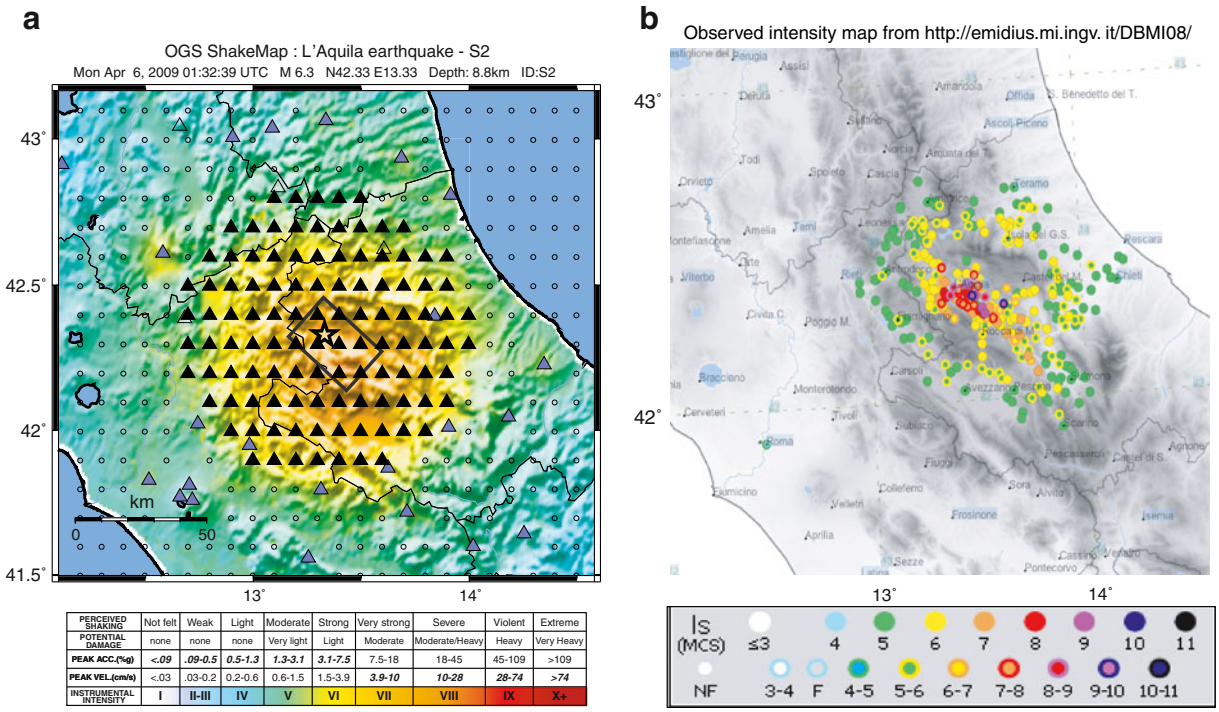

Fig. 9 **a** Instrumental MCS intensity ShakeMap for test S2. The *blue triangles* are the INGV broadband station, while the *black ones* are sites where the synthetics have been computed. **b** Observed macroseismic intensities downloaded from the DBMI08aq (2009) database

computed on a regular grid around the epicenter can lead to an improvement of shaking maps.

Our findings, related to the L'Aquila earthquake, can be certainly generalized beyond this particular case study. Recorded data are the irreplaceable ingredient to obtaining accurate shaking maps soon after an earthquake, but in the case where any near-source data are missing, the integration of observations with synthetics improves the ShakeMap performance.

Since the shakemaps must be generated as fast as possible for Civil Defense purposes, proper algorithms and some approximations are needed. In this regard, the procedure that we applied sounds promising for near real-time application since it provides a rough finite source model and synthetic seismograms in a short time. Furthermore, being based on open-source software, it can be easily implemented in earthquake-prone areas where the station coverage is poor.

However, the application in real time is possible only after the whole procedure is tuned for a specific region. In principle, every step can operate in an automatic mode, but some programming work is still needed. As mandatory prerequisites, the ShakeMap software must be properly customized for the region under investigation together with a well-calibrated velocity model and a robust moment tensor solution computed in real time.

7 Data and Resources

Regional and local data were recorded by the OGS (Bragato et al. 2011), INGV (Amato and Mele 2008), and RAN (Zambonelli et al. 2011) networks. PGA values were downloaded from the ITACA database (http://itaca.mi.ingv.it). The facilities of the IRIS Data Management Center were used for access to teleseismic data. Moment tensor was computed using the *tdmt_invc* package (Dreger 2003) (Green's functions were computed using the FKRPROG software developed by Chandan Saikia). The Teleseismic Body-Wave Inversion program by Kikuchi and Kanamori (2003) was employed for slip distribution retrieval. The maps were produced using GMT software (Wessell and Smith 1991).

Acknowledgments We are grateful to Alberto Michelini and Licia Faenza for kindly providing us the data used to generate the ShakeMaps, and to Pier Luigi Bragato for his technical assistance. Thomas Braun, Alberto Michelini, and an anonymous reviewer are acknowledged for their constructive criticism, which helped in improving this paper. This research has benefited from funding provided by the Italian Presidenza del Consiglio dei Ministri–Dipartimento della Protezione Civile (DPC) under the contract 2007–2009 DPC-S3. Scientific papers funded by DPC do not represent its official opinion and policies.

References

Akkar S, Bommer JJ (2007a) Empirical prediction equations for peak ground velocity derived from strong-motion records from Europe and the Middle East. Bull Seismol Soc Am 97:511–530

Akkar S, Bommer JJ (2007b) Prediction of elastic displacement response spectra in Europe and the Middle East. Earthquake Engng Struct Dyn 36:1275–1301

Amato A, Mele F (2008) Performance of the INGV National Seismic Network from 1997 to 2007. Ann Geophys 51:417–431

Ameri G, Massa M, Bindi D, D'Alema E, Gorini A, Luzi L, Marzorati S, Pacor F, Paolucci R, Puglia R, Sferzini C (2009) The 6 April 2009, Mw 6.3, L'Aquila (Central Italy) earthquake: strong-motion observations. Seism Res Lett 80:951–966

Ameri G, Cirella A, Cultrera G, Faenza L, Herrero A, Pacor F, Piatanesi A, Saraò A, Spagnuolo E, Emolo A (2010) Testing the improvement of ShakeMaps using finite-fault models and synthetic seismograms. European Seismological Commission (ESC) 32nd General Assembly, Sept. 6–10, Montpellier, France. Abstract vol, p. 215

Anzidei M, Boschi E, Cannelli V, Devoti R, Esposito A, Galvani A, Melini D, Pietrantonio G, Riguzzi F, Sepe V, Serpelloni E (2009) Coseismic deformation of the destructive April 6, 2009 L'Aquila earthquake. Geophy Res Lett 36:L17307. doi:10.1029/2009GL039145

Atkinson GM, Boore DM (2006) Earthquake ground-motion prediction equations for eastern North America. Bull Seismol Soc Am 96:2181–2205

Atkinson GM, Boore DM, Assatourians K, Campbell KW, Motazedian D (2009) A guide to differences between stochastic point source and stochastic finite fault simulations. Bull Seismol Soc Am 99:3192–3201

Atzori S, Hunstad I, Chini M, Salvi S, Tolomei C, Bignami C, Stramondo S, Trasetti E, Antonioli A, Boschi E (2009) Finite fault inversion of DInSAR Coseismic displacement of the 2009 L'Aquila earthquake (Central Italy). Geophys Res Lett 36:L15305. doi:10.1029/2009GL039293

Barani S, De Ferrari R, Ferretti G, Spallarossa D (2009) Calibration of soil amplification factors for real time ground motion scenarios in Italy and comparison with experimental data from L'Aquila sequence. Progetti convenzione DPC-INGV 2007–2009. 1st annual meeting, Rome, 19–21 October 2009

Beresnev I, Atkinson GM (1998) Stochastic finite-fault modeling of ground motions from the 1994 Northridge, California, earthquake. I. Validation on rock sites. Bull Seismol Soc Am 88:1392–1401

Bindi D, Pacor F, Luzi L, Massa M, Ameri G (2009) The Mw 6.3, 2009 L'Aquila earthquake: source, path and site effects from spectral analysis of strong motion data. Geophys J Int 179:1573–1579

Boncio P, Pizzi A, Brozzetti F, Pomposo G, Lavecchia G, Di Naccio D, Ferrarini F (2010) Coseismic ground deformation of the 6 April 2009 L'Aquila earthquake (central Italy, Mw6.3). Geophys Res Lett 37:L06308. doi:10.1029/2010GL042807

Boore DM (1983) Stochastic simulation of high-frequency ground motions based on seismological models of the radiated spectra. Bull Seismol Soc Am 79:1865–1894

Boore DM (2005) SMSIM—Fortran Programs for Simulating Ground Motions from Earthquakes: Version 2.3—A revision of OFR 96-80- A, U.S. Geol. Surv. Open-File Report 00 509, revised 15 August 2005, pp. 55. Available from the online publications link on http://www.daveboore.com/ Last access september 2011

Boore DM (2009) Comparing stochastic point-source and finite-source ground motion simulations: SMSIM and EXSIM. Bull Seismol Soc Am 99:3202–3216

Borcherdt T (1994) Estimates of site-dependent response spectra for design (methodology and justification). Earthq Spectra 10:617–654

Bragato PL (2009) Assessing regional and site-dependent variability of ground motions for ShakeMap implementation in Italy. Bull Seism Soc Am 99:2950–2960

Bragato PL, Di Bartolomeo P, Pesaresi D, Plasencia Linares MP, Saraò A (2011) Acquiring, archiving, analyzing and exchanging seismic data in real time at the Seismological Research Center of the OGS in Italy. Annals Geophysics 54:67–75

Castro RR, Pacor F, Franceschina G, Bindi D, Zonno G, Luzi L (2008) Stochastic strong-motion simulation of the Mw 6 Umbria–Marche earthquake of September 1997: comparison of different approaches. Bull Seismol Soc Am 98:662–670

Cirella A, Piatanesi A, Cocco M, Tinti E, Scognamiglio L, Nichelini A, Lomax A, Boschi E (2009) Rupture history of the 2009 L'Aquila (Italy) earthquake from non-linear joint inversion of strong motion and GPS data. Geophys Res Lett 36:L19304. doi:10.1029/2009GL039795

DBMI08aq (2009) INGV—database macrosismico italiano. http://emidius.mi.ingv.it/DBMI08 Last Accessed Aug 2011

Di Bona M, Lucente FP, Piana Agostinetti N (2008) Crustal structure and Moho depth profile crossing the central Apennines (Italy) along the N42° parallel. J Geophys Res 113:B12306. doi:10.1029/2008JB005625

Douglas J (2007) Inferred ground motions on Guadeloupe during the 2004 Les Saintes earthquake. Bull Earthq Eng 5:363–376

Dreger DS (2003) TDMT_INV: Time domain seismic moment tensor INVersion. In: Lee et al (ed) International handbook of earthquake and engineering seismology. Part B. International Geophysics Series. Academic Press, Amsterdam, pp. 1627–1628

Faenza L, Michelini A (2010) Regression analysis of MCS intensity and ground motion parameters in Italy and its application in ShakeMap. Geophys J Int 180:1138–1152

Faenza L, Lauciani V, Michelini A (2011) Rapid determination of the shakemaps for the L'Aquila main shock: a critical analysis. Boll Geof Teor Appl 52(3):407–425. doi:10.4430/bgta0020

Gallipoli MR, Mucciarelli M (2009) Comparison of site classification from VS30, VS10, and HVSR in Italy. Bull Seismol Soc Am 99:340–351

Herrmann RB (1985) An extension of random vibration theory estimates of strong ground motion to large earthquakes. Bull Seismol Soc Am 75:1447–1453

Herrmann RB, Malagnini L, Munafò I (2011) Regional moment tensors of the 2009 L'Aquila Earthquake sequence. Bull Seism Soc Am 101:975–993

Hok S, Wald DJ (2003) Spatial variability of peak strong ground motions: implications for ShakeMap interpolations. EOS. Trans. AGU, 84(46), Fall Meet. Suppl Abstract S51E-0092

ITACA Working Group (2010) Data base of the Italian strong motion records: http://itaca.mi.ingv.it Last Accessed September 2011

Kikuchi M, Kanamori H (1982) Inversion of complex body waves. Bull Seismol Soc Am 72:491–506

Kikuchi M, Kanamori H (1993) Source complexity of the 1988 Armenian earthquake: evidence for a slow after-slip event. J Geophys Res 98:15797–15808

Kikuchi M, Kanamori H (2003) Note on teleseismic body-wave inversion program. http://www.eri.u-tokyo.ac.jp/ETAL/KIKUCHI/ Last Accessed September 2011

Lin KW, Wald DJ, Worden B, Shakal AF (2005) Quantifying CISN Shakemap uncertainties. Proceedings of the Eighth U.S. National Conference on Earthquake Engineering Paper no. 1482

Mazza S, Olivieri M, Mandiello A, Casale P (2008) The Mediterranean Broad Band Seismographic Network Anno 2005/06, Earthquake Monitoring and Seismic Hazard Mitigation in Balkan Countries, NATO Science series 81:133–149. doi:10.1007/978-1-4020-6815

Maugeri M, Simonelli AL, Ferraro A, Grasso S, Penna A (2011) Recorded ground motion and site evaluation for the April 6, 2099 L'Aquila earthquake. Bull Earthquake Eng 9:157–179

Mavroeidis GP, Papageorgiou AS (2003) A mathematical representation of near-fault ground motions. Bull Seismol Soc Am 93:1099–1131

Michelini A, Faenza L, Lauciani V, Malagnini L (2008) ShakeMap implementation in Italy. Seism Res Lett 79:688–697

Moratto L, Costa G, Suhadolc P (2009) Real-time generation of ShakeMaps in the Southeastern Alps. Bull Seismol Soc Am 99:2489–2501

Motazedian D, Atkinson GM (2005) Stochastic finite-fault modeling based on a dynamic corner frequency. Bull Seismol Soc Am 95:995–1010

Panza GF, Saraò A (2000) Monitoring volcanic and geothermal areas by full seismic moment tensor inversion: are non-double couple components always artefacts of modelling? Geophys J Int 143:353–364

Parotto M, Cavinato GP, Miccadei E, Tozzi M (2003) Line CROP 11: Central Apennines. In: Scrocca D, Doglioni C, Innocenti F, Manetti P, Mazzotti A, Bertelli L, Burbi L, D'Offizi S (eds) CROP Atlas: seismic reflection profiles of the Italian crust (Memorie Descrittive della Carta Gologica d'Italia, LXII) 62:145–153

Pino NA, Di Luccio F (2009) Source complexity of the 6 April 2009 L'Aquila (central Italy) earthquake and its strongest aftershock revealed by elementary seismological analysis. Geophys Res Lett 36:L23305. doi:10.1029/2009GL041331

Poiata N, Kazuki K, Vuan A, Miyake H (2011) Broadband source model for 2009 L'Aquila, Italy earthquake. Proceedings of 8th International Conference on Urban Earthquake Engineering March 7–8, 2011, Tokyo Institute of Technology, Tokyo, Japan

Pondrelli S, Salimbeni S, Morelli A, Ekstrom G, Olivieri M, Boschi E (2010) Seismic moment tensors of the April 2009, L'Aquila (central Italy), earthquake sequence. Geophys J Int 180:238–242, Herma

Roumelioti Z, Kiratzi A, Theodulidis N (2004) Stochastic strong ground-motion simulation of the 7 September 1999 Athens (Greece) earthquake. Bull Seismol Soc Am 94:1036–1052

Saraò A (2007) Seismic moment tensor determination at CRS: feasibility study. Open Report, OGS 2007/60-CRS/16. OGS, Trieste, pp. 43

Scognamiglio L, Tinti E, Michelini A, Dreger D, Cirella A, Cocco M, Mazza S, Piatanesi A (2010) Fast determination of moment tensors and rupture history: what has been learned from the 6 april 2009 L'Aquila earthquake sequence. Seismol Res Lett 81:892–906

Ugurhan B, Askan A (2010) Stochastic strong ground motion simulation of the 12 November 1999 Düzce (Turkey) earthquake using a dynamic corner frequency approach. Bull Seismol Soc Am 100:1498–1512

Wald LA, Mori J (2000) Evaluation of methods for estimating linear site-response amplifications in the Los Angeles region. Bull Seism Soc Am 90:S32–S42

Wald DJ, Quitoriano V, Heaton TH, Kanamori H, Scrivner CW, Worden CB (1999) TriNet "ShakeMaps": rapid generation of peak ground motion and intensity maps for earthquakes in Southern California. Earthq Spectra 15:537–555

Wald DJ, Worden CB, Quitoriano V, Pankow KL (2006) ShakeMap Manual: technical manual, user's guide, and software guide, version 1.0 6/19/06, 1–156. http://pubs.usgs.gov/tm/2005/12A01/ Last Accessed September 2011

Wells DL, Coppersmith KJ (1994) New empirical relationships among magnitude, rupture length, rupture width, rupture area, and surface displacement. Bull Seismol Soc Am 84:974–1002

Wessell P, Smith WHF (1991) Free software helps map and display data. EOS Trans AGU 72:441

Zambonelli E, De Nardis R, Filippi L, Nicoletti M, Dolce M (2011) Performance of the Italian strong motion network during the 2009, L'Aquila seismic sequence (central Italy). Bull Earthquake Eng 9:39–65